
PLA4D: Pixel-Level Alignments for Text-to-4D Gaussian Splatting

Qiaowei Miao
Zhejiang University

Yawei Luo*
Zhejiang University

Yi Yang
Zhejiang University

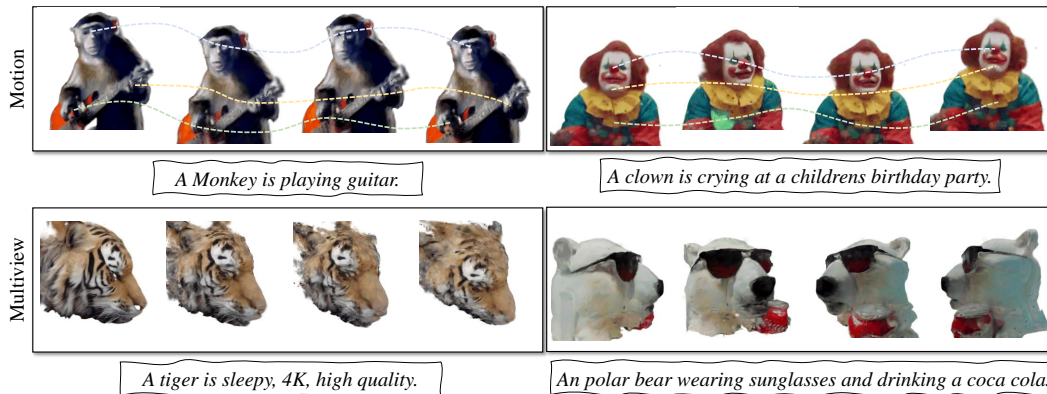


Figure 1: Text-to-4D synthesis results of our PLA4D. Top: we show the motion sequences of the 4D targets. Dotted lines represent the motion trajectories controlled by the deformation network at different timesteps. Bottom: we present the multiple views of 4D objects at one timestep.

Abstract

As text-conditioned diffusion models (DMs) achieve breakthroughs in image, video, and 3D generation, the research community’s focus has shifted to the more challenging task of text-to-4D synthesis, which introduces a temporal dimension to generate dynamic 3D objects. In this context, we identify Score Distillation Sampling (SDS), a widely used technique for text-to-3D synthesis, as a significant hindrance to text-to-4D performance due to its Janus-faced and texture-unrealistic problems coupled with high computational costs. In this paper, we propose **Pixel-Level Alignments for Text-to-4D Gaussian Splatting (PLA4D)**, a novel method that utilizes text-to-video frames as explicit pixel alignment targets to generate static 3D objects and inject motion into them. Specifically, we introduce Focal Alignment to calibrate camera poses for rendering and GS-Mesh Contrastive Learning to distill geometry priors from rendered image contrasts at the pixel level. Additionally, we develop Motion Alignment using a deformation network to drive changes in Gaussians and implement Reference Refinement for smooth 4D object surfaces. These techniques enable 4D Gaussian Splatting to align geometry, texture, and motion with generated videos at the pixel level. Compared to previous methods, PLA4D produces synthesized outputs with better texture details in less time and effectively mitigates the Janus-faced problem. PLA4D is fully implemented using open-source models, offering an accessible, user-friendly, and promising direction for 4D digital content creation. Our project page: <https://miaoqiaowei.github.io/PLA4D>.

*Corresponding author.

1 Introduction

Text-to-4D content generation holds immense potential across diverse applications, including game production and autonomous driving. Currently, the task remains highly challenging due to the need for high-quality geometry and texture generation alongside coherent object animations. Despite numerous efforts [8; 9; 39; 20; 26; 38; 34] focused on enhancing 3D generation quality and efficiency, these methods lack support for dynamic motions. Recent advancements in video generation [41; 5; 2; 50; 1; 49] offer temporal motion information. However, there is still a considerable research gap in integrating motion cues from videos to achieve 4D generation tasks for dynamic 3D objects.

Most of the existing text-to-4D synthesis methods [42; 3] are represented by using Neural Radiance Fields (NeRF) [32]. By combining the ability of video generative model [41], MAV3D [42] achieves text-to-4D generation by distilling text-to-video diffusion models (DMs) on a Hexplane [6]. Employing a hybrid score distillation sampling (SDS), 4D-fy [3] achieves compelling text-to-4D generation based on multiple pre-trained diffusion models. Recently, a text-to-4D generation work named AYG [27] is constructed based on 3D Gaussians simulated by a deformation network. The key modules of AYG include SDS across text-to-image DM [39], text-to-multiview-image DM [39] and text-to-video DM [5]. A commonality among these modules is their heavy reliance on SDS to provide priors for guiding the generation of geometry, texture, and motion.

Nevertheless, several notable issues inherent in SDS, such as Janus faces, unrealistic textures, and high computational costs [45; 27; 42; 34; 36; 39; 51; 44; 56], pose significant challenges to text-to-4D performance: Injecting motion guidance into flawed 3D representations can further degrade 4D visual perception, while the necessity of handling multi-frame video exacerbates the time-consuming nature of SDS. To reduce the Janus-face problem, MVDream [39] fine-tunes the stable diffusion [37] on the object-centric 3D dataset Objaverse [11; 10] and provides a strong 3D prior for SDS. However, the generated products are under the conditions of four fixed camera views (0° , 90° , 180° , 270°), which involves viewpoint bias that will force random view-rendered images to align with the known view conditions (*i.e.*, and 20° rendered image could be regarded as the image got from 0°). The following works [27; 42; 36; 51; 44; 56] often directly employ such pre-trained multi-view DMs [39] without extra modifications, inevitably perpetuating the same problem.

In this paper, we introduce a novel framework for Text-to-4D content creation, dubbed PLA4D (Pixel-Level Alignments for Text-to-4D Gaussian Splatting), which capitalizes on pixel-level alignments to guide the generation process based on 3D Gaussian Splatting (3DGS) [23]. **Firstly**, PLA4D utilizes a text-to-video model to generate a sequence of frames serving as pixel alignment targets for geometry, texture, and motion. **Secondly**, PLA4D is designed to obtain high-quality static 3D Gaussians based on the frame sequence. Starting with the first frame, a feed-forward model transforms it into a mesh. Such mesh is utilized for training 3D Gaussians through our new proposed process called GS-Mesh contrastive learning. It offers intuitive geometric guidance for 3DGS from the mesh, circumventing the slow distillation in DMs. To address the overly smooth issue in images rendered from mesh, we align the rendered images with the generated frames to enhance texture details. Compared to SDS-based methods [27; 36; 56], the explicit geometric priors provided by the mesh effectively alleviate the multi-head issue. Additionally, applying pixel alignment between GS-rendered images, mesh-rendered images, and video frames reduces the training time from hours [27; 36; 3; 56] to around ten minutes. **Finally**, PLA4D builds a deformation network to activate the static 3D Gaussian. The deformation network controls the displacement of each Gaussian at each timestep to match the poses in the generated video. However, such displacement is prone to disrupt the 3D object’s surface. To mitigate this, we propose a reference refinement method that uses multiview diffusion priors to inpaint cavities within the object.

We identify that PLA4D can generate a wide range of dynamic scenes rapidly, producing diverse, vivid, and intricate details while maintaining 3D consistency, as shown in Fig. 1. In summary, our contributions are as follows:

- We propose PLA4D, a novel text-to-4d generation framework with explicit pixel-level alignments.
- We propose GS-Mesh contrastive learning and focal alignment, which learns geometry consistency from mesh and yields textures as fine as those in the generated video frames.
- For accurate motion extraction, we present a novel motion alignment method and reference refinement technology to optimize dynamic surfaces.

- Without bells and whistles, PLA4D achieves remarkable performance, generating 4D scenes with fine textures, accurate geometry, and coherent motion in significantly less time.

2 Related work

3D Content Generation. Recent advancements in diffusion models within 2D domains have sparked significant interest in exploring 3D generative modeling [8; 9; 12; 13; 20; 22; 25; 26; 31; 43; 46; 47; 7] for content generation. Under given control conditions (*e.g.*, text prompt or single image), some efforts [39; 29; 38; 28; 30] are made to extend 2D diffusion models from single-view images to multi-view images to seamlessly integrate with different 3D representation methods (*e.g.* Nerf [32], Mesh [19], and 3D Gaussian Splatting [23]). However, due to the uncertainty of the diffusion model’s denoise process, the multi-view consistency and corresponding camera poses of generated images are not guaranteed, leading to artifacts and texture ambiguity in the generated 3D object. Further, some works [34; 51; 48] apply score distillation sampling (SDS) in latent space to extend the 2D diffusion models to guide 3d generation. Although such SDS-based methods can improve the textural of 3D representation, they frequently suffer from multi-face Janus issues due to the lack of comprehensive multi-view knowledge or 3D awareness during score distillation. More recently, some methods [26; 23; 9; 31] have integrated the above two approaches, which use pre-trained multi-view diffusion for SDS. The comprehensive multiview knowledge or 3D awareness hidden in the pre-trained model enhances the consistency of 3D representation, yet such SDS-based optimization methods are time-consuming needing hours to train.

Video Generation. Video generation [1; 5; 14; 15; 16; 17; 24; 4], including text-to-video and image-to-video generation, has been getting more and more attention recently. The former, such as MAV [41] and AYL [5], rely on large amounts of high-quality text-to-video data for training to deepen their understanding of verbs, enabling them to generate rich and creative sequences of coherent video frames. The latter [16; 4] infers subsequent actions of the target object based solely on a given initial frame image, which does not support flexible control over actions.

4D Content Generation. At the current stage, the quality of 4D generation highly relies on 3D generation and video generation. It tests the geometric and textural quality of the generated objects and requires coherence in temporal actions. Satisfying both conditions simultaneously is very challenging, hence 4D generation tasks were previously overlooked. Dream-in-4D [56] developed a new text-to-4D synthesis scheme. In contrast to PLA4D, the work leverages a NeRF-based 4D representation and focuses on image-guided and personalized generation, instead of using dynamic 3D Gaussians and targeting temporally extended generation as well as the possibility to easily compose different 4D assets in large scenes. Most related to PLA4D is AYG [27], the only text-to-dynamic 4D scenes with Gaussian splitting to the best of our knowledge. AYG proposes a pipeline that mainly relies on the SDS of text-to-image diffusion, text-to-video diffusion, and text-to-multiview diffusion models. However, the Janus-face problem is commonly encountered in generated products which can not be reduced by their view guidance method.

Other related works, such as Animate124 [55] and DreamGaussian4D [36], are image-to-4D models that use an image-to-video diffusion model to expand the temporal dimension for static objects. Image-driven motion guidance is hard to compare to the creations generated by text-driven methods. Besides, image-driven methods need powerful generalization to predict correct motions based on unseen images, especially if other diffusion models generate the given image. PLA4D outperforms AYG and DreamGaussian4D quantitatively and synthesizes significantly higher-quality 4D scenes, without excessive time expenditure and Janus-face problem. Besides, during object motion, surface tearing, as seen in other Gaussian splash methods, does not occur by using PLA4D. PLA4D breaks away from dependency on closed-source models [41; 5] through innovative design, achieving superior performance. Its flexible architecture provides more avenues for 4D GS tasks.

3 Methodology

We detail PLA4D as follows. First, we introduce the necessary preliminaries in Sec. 3.1. Then, in Sec. 3.2, we present the pipeline overview of PLA4D. PLA4D employs an open-source text-to-video diffusion model to generate video. Based on the generated video, we implement frame-to-3D generation in Sec. 3.3. Finally, in Sec. 3.4, we introduce our 3D-to-4D generation method.

3.1 Preliminaries

3D Gaussian Splatting (3DGS) [23] represents a 3D scene involves a collection of N Gaussian points, each defined by four attributes: positions μ_i , covariances Σ_i , colors ℓ_i , and opacities α_i . To render novel views, 3DGS reprojects the 3D Gaussians onto a 2D image space, obtaining their projection positions μ and corresponding covariances $\hat{\Sigma}_i$. Point-based α -blending rendering [57] is then applied to determine the color $\mathcal{C}(p)$ of image pixel p along a ray r . This rendering process is outlined as follows:

$$\mathcal{C}(p) = \sum_{i \in N} \ell_i \eta_i \prod_{j=1}^{i=1} (1 - \eta_j), \quad \eta_i = \alpha_i \exp \left[-\frac{1}{2} (p - \hat{\mu}_i)^T \hat{\Sigma}_i (p - \hat{\mu}_i) \right], \quad (1)$$

where j iterates over the points traversed by the ray r , ℓ_i and α_i donate the color and opacity of the i -th Gaussian. $\hat{\mu}_i$ is the projection of μ_i on 2D image plane. Throughout the training process, 3DGS employs an adaptive control mechanism to enhance representation quality. This method involves filtering and densifying Gaussian points based on their transparency at regular intervals. Notably, 3D Gaussians constitute the foundational 3D representation utilized within the framework of PLA4D.

Score Distillation Sampling (SDS) is widely used in 3D generation methods [39; 34; 36; 39; 51], which aligns the 3D generation process to the 2D diffusion models (DMs) training process. In the forward process of 2D DMs, sample noise ϵ from $q(x)$ and add it on the data x (e.g., images and videos) with t times until $q(x_t)$ converges to a Gaussian prior distribution $\mathcal{N}(0, \mathbf{I})$. In the reverse process, the network θ is trained to predict the removal noise $\hat{\epsilon}$ for denoising and reconstructing data x . 3D generation methods set the renderings got from 3D scene representation as data x , and calculate the Mean Squared Error (MSE) to get SDS gradient [34]:

$$\nabla_{\theta} \mathcal{L}_{\text{SDS}}(x = g(\theta)) = \mathbb{E}_{t, \epsilon} \left[w(t) (\hat{\epsilon}_{\phi}(z, v, t) - \epsilon) \frac{\partial x}{\partial \theta} \right], \quad (2)$$

where t is the timestamp of denoising process, and $w(t)$ is time-dependent weights. z represents the latent of x needing to denoise. v indicates the given conditions, such as text prompts and images. The SDS gradients are then propagated backward through the differentiable rendering process g into the 3D scene representation and update its parameters θ .

SDS is notoriously known to cause the Janus-face problem and long-time cost [34; 39; 51]. In 2D DMs, a common technology named Classifier-Free Guidance [18] (CFG), which trains the 2D DMs in both conditional and unconditional modes [53], *i.e.*, estimates both $\nabla_x \log q(x|v)$ and $\nabla_x \log q(x)$. Correspondingly, it can be expressed as $\hat{\epsilon}(z, v, t)$ and $\hat{\epsilon}(z, t)$. With CFG, the removal noise $\hat{\epsilon}$ is modified as: $\hat{\epsilon}_{\phi}(z, v, t) \rightarrow \hat{\epsilon}_{\phi}(z, v, t) + \omega [\hat{\epsilon}_{\phi}(z_t, v, t) - \hat{\epsilon}_{\phi}(z_t, t)]$, where ω controls the trade-off between fidelity and diversity. To simplify, we donate the $\hat{\epsilon}_{\phi}(z_t, v, t) - \epsilon$ as δ_x . So the δ_x with CFG can be represented as:

$$\delta_x = \underbrace{[\hat{\epsilon}_{\phi}(z_t, v, t) - \epsilon]}_{\delta_x^{\text{pix}}} + \omega \cdot \underbrace{[\hat{\epsilon}_{\phi}(z_t, v, t) - \hat{\epsilon}_{\phi}(z_t, t)]}_{\delta_x^{\text{cond}}}. \quad (3)$$

The terms δ_x^{pix} and δ_x^{cond} respectively signify the descent directions aligned with pixels x and semantics of condition v . Here, the parameter θ of the DM is crucial but often overlooked, which is the key factor causing the Janus-face problem and extensive time expenditure. Specifically, DMs [37; 39; 29; 38] are trained with images captured from a few or even single perspective c , which is implicitly introduced into ϕ and as the priors for SDS. So, optimizing SDS loss with image rendered from a random viewpoint \hat{c} is equivalent to minimizing $\text{KL}(q(z_t|x = g(\theta, \hat{c})) || p_{\phi}(z_t|v, c))$. This implies that the 3D scene representation θ learns a prior by aligning different random viewpoints \hat{c} to fixed and limited viewpoints c , which leads to the Janus-face problem. Regarding time cost, several researchers [34; 42; 3; 55] indicate that SDS requires a significant amount of time for optimization. Let us refocal on Eq. 2. SDS loss can be regarded as a method to push the renderings' latent z_t into the latent space of DMs. However, all parameters of DMs are frozen, and only the parameter ϕ in Eq. 2 is learnable. That means the training process requires the frozen DMs' denoisers to predict correct removal noise $\hat{\epsilon}$ at each timestamp t from any arbitrary viewpoint c . Thus, SDS needs an amount of time expenditure for 3D generation.

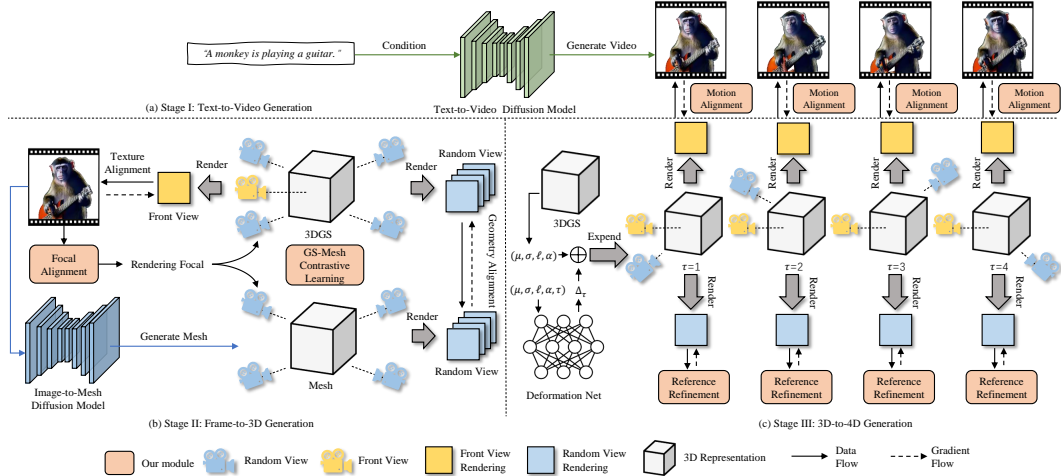


Figure 2: Pipeline of PLA4D. (I) Text-to-Video generation: generating video as the pixel-level alignment targets for 3D and 4D content. (II) Frame-to-3D generation: applying GS-Mesh contrastive learning and focal alignment for texture and geometry alignment, which constructs static 3D Gaussians with correct geometry and detailed texture based on the first frame. (III) 3D-to-4D generation: PLA4D employs motion alignment and reference refinement methods to inject motion into 3D Gaussians.

3.2 Pipeline Overview

PLA4D’s pipeline comprises three stages: text-to-video generation, frame-to-3D generation, and 3D-to-4D generation, as shown in Fig. 2. (I) Given the text prompt, PLA4D uses an open-source text-to-video DM to generate video first. This video, possessing detailed textures and smooth motions, serves as the alignment target for 3D generation and 4D synthesis. (II) Based on the first frame of the generated video, PLA4D extends it to a 3D object with fine textures and accurate geometry. Therefore, we align the front-view rendered image of 3DGS to the frame to save detailed textures called texture alignment. However, due to the inaccurate frame-focal pair, rigid alignment may result in massive of the 3D object. To solve this problem, we propose the *Focal Alignment* method to search for the best rendering focal thus better aligning the rendered image to the frame. Additionally, we perform *GS-Mesh Contrastive Learning* by aligning the random rendered results of 3DGS and Mesh to capture the texture and geometry accurately and precisely. (III) Furthermore, we construct a deformation net to predict the changes of each point at each timestamp for injection motions. Therefore, we propose the *Motion Alignment* on the front view to push the rendered frames of dynamic 3D objects to the target video. For a better surface representation, we introduce an additional *Reference Refinement* method to optimize 4D objects.

3.3 Frame-to-3D Generation

Focal Alignment. PLA4D aims to use text-guided synthetic video as the pixel-level alignment targets for 3D and 4D generation, which needs a matched focal for frames. However, the multiple-step denoising process of DMs introduces uncertainty to the frames, which makes $\{I_{\text{vid}}^{\tau}\}_{\mathcal{T}}$ ’s corresponding focal is not equal to the settings used in DMs’ pretraining process. Therefore, we propose focal alignment to search for the matched focal f' . Specifically, we start with the video synthesis. Given the text prompt v , PLA4D applies a text-to-video DM G_{vid} to creates a video $\{I_{\text{vid}}^{\tau}\}_{\mathcal{T}} = G_{\text{vid}}(\epsilon; v)$ with \mathcal{T} frames. The ϵ is the random noise. Because the view angles in the generated frames are relatively fixed, we set the video’s view c as the 3D object’s front perspective. Next, we need to construct a 3D object and compare its front view rendering and I_{vid}^1 to search f' , as shown in Fig. 3(a). Hence, we introduce CRM [52], an image-to-mesh feed-forward 3D generation model, to furnish a mesh representation ψ as the initialization of 3D Gaussians θ . We render ψ ’s front-view images $\{x_{\psi}\}_M$ with M different focals iterated from $f + \Delta f_{\text{min}}$ to $f + \Delta f_{\text{max}}$. We calculate the MSE between

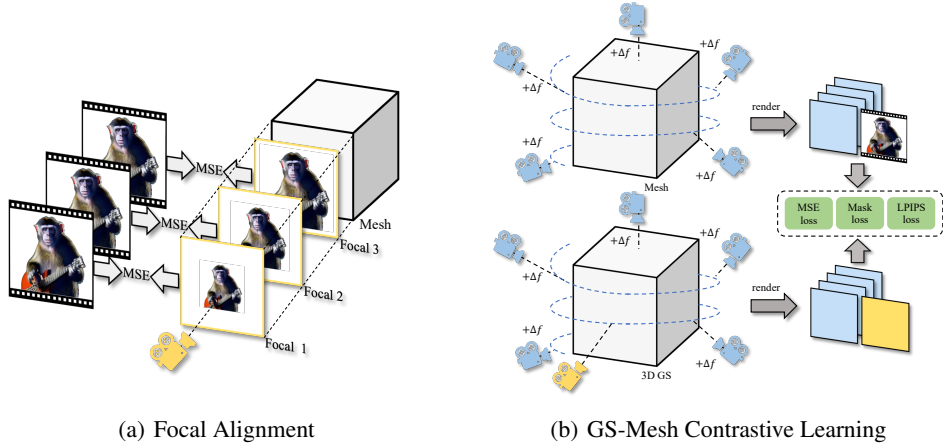


Figure 3: Focal alignment and GS-Mesh contrastive learning in frame-to-3D stage. (a) We render multiple front-view images and calculate the MSE with the first frame for searching the matched focal. (b) We collect two sets of images: one of 3D Gaussians and another of mesh renderings, both captured using the same random camera poses. We include the first generated frame and the front-view rendering in these two sets. Then, we calculate the MSE loss, Mask loss, and LPIPS loss between the corresponding images from these sets.

I_{vid}^1 and $\{x_\psi\}_M$ for searching the matched focal f' :

$$f' = \arg \min_f \sum_{H,W} \|x_\psi^f - I_{\text{vid}}^1\|_2^2. \quad (4)$$

For ease of understanding, in the following sections, we donate f as the matched focal f' .

GS-Mesh Contrastive Learning. With the corresponding focal f , we propose GS-Mesh contrastive learning to align the front-view 3DGS renderings to the frames to achieve texture alignment, which is composed of three losses: (I) \mathcal{L}_{MSE} for aligning the pixel-level similarity, (II) $\mathcal{L}_{\text{Mask}}$ for reducing the floaters, and (III) $\mathcal{L}_{\text{LPIPS}}$ for enhancing the visual perceptual perception. In particular, we use the MSE loss between front view c rendering x_θ of 3D Gaussians and I_{vid}^1 as follows:

$$\mathcal{L}_{\text{MSE}}(x_\theta^c, I_{\text{vid}}^1) = \sum_{H,W} \|x_\theta^c - I_{\text{vid}}^1\|_2^2. \quad (5)$$

Besides, to reduce the floaters, we also use the transparent output α of 3D Gaussians as the mask and calculate the mask loss:

$$\mathcal{L}_{\text{Mask}}(x_\theta^c, I_{\text{vid}}^1) = \sum_{H,W} \|\alpha_\theta^c - \alpha_{\text{vid}}^1\|_2^2, \quad (6)$$

where α_{vid}^1 is the alpha channel of I_{vid}^1 . Besides, we introduce Learned Perceptual Image Patch Similarity (LPIPS) [54], which is a metric used to measure perceptual differences between images. We apply LPIPS loss between x_θ^c and I_{vid}^1 to enhance the visual quality of textures. $\mathcal{L}_{\text{LPIPS}}$ needs an encoder (*i.e.*, VGG [40]) to extract feature stack from l layers and unit-normalize in the channel dimension, and calculate the MSE between features extracted from each layer:

$$\mathcal{L}_{\text{LPIPS}}(x_\theta^c, I_{\text{vid}}^1) = \sum_l \frac{1}{H_l W_l} \sum_{h,w} \|z_\theta^c - z_{\text{vid}}^1\|_2^2. \quad (7)$$

Now, we can get the texture alignment loss \mathcal{L}_{TA} :

$$\mathcal{L}_{\text{TA}} = \lambda \mathcal{L}_{\text{MSE}}(x_\theta^c, I_{\text{vid}}^1) + \lambda \mathcal{L}_{\text{Mask}}(x_\theta^c, I_{\text{vid}}^1) + \gamma \mathcal{L}_{\text{LPIPS}}(x_\theta^c, I_{\text{vid}}^1), \quad (8)$$

where λ is the training step-depend coefficient, and γ is scaling weight for balance.

As mentioned above, using multiview DMs for SDS could implicitly introduce perspective bias, which is hidden in their pre-trained weights and causes Janus-face problems. Here, we propose

geometry alignment for learning multi-view consistency. Specifically, we use 3DGS θ and mesh ψ as references for contrastive learning, as shown in Fig. 3(b). We randomly choose $N_{c'}$ camera poses $\{c'_i\}_{N_{c'}}$, and each corresponding focal is $f + \Delta f$, Δf is a slight and random perturbation. Different from multiview DMs’ productions, the rendered images of mesh ψ are obtained from one entity, that naturally has multiview consistency. Besides, this method can provide references from any number of different viewpoints for training 3DGS θ , such density data can avoid artifacts in renderings. The geometry alignment loss \mathcal{L}_{ge} can be summary as:

$$\mathcal{L}_{GA} = \sum_{i=1}^{N_{c'}} \lambda \mathcal{L}_{\text{MSE}}(x_{\theta}^{c'_i}, x_{\psi}^{c'_i}) + \lambda \mathcal{L}_{\text{Mask}}(x_{\theta}^{c'_i}, x_{\psi}^{c'_i}) + \gamma \mathcal{L}_{\text{LPIPS}}(x_{\theta}^{c'_i}, x_{\psi}^{c'_i}). \quad (9)$$

Overall, the 3D loss $\mathcal{L}_{3D} = \mathcal{L}_{TA} + \mathcal{L}_{GA}$ is set as the optimization target to train 3DGS θ .

3.4 3D-to-4D Target Generation

While in Sec. 3.3, we only optimize the 3DGS. In Sec. 3.4, we construct a deformation field Φ [33; 35] and only optimize Φ for extracting and injecting motion by adding temporal dimension τ for static 3DGS. To achieve this goal, we propose motion alignment and reference refinement methods.

Motion Alignment. The deformation net Φ is a multilayer perception (MLP) network Φ trained to predict the change Δ_t of position, rotation, scale, and opacity of each Gaussian given timestamp τ . As shown in Fig. 2 (c), the new attribute S' for each Gaussian p can be calculated by $S' = S + \Delta_t$. Based on these Gaussian points, we can render the image $x_{\theta}^{c',\tau}$ corresponding to the time τ . Here, we minimize the motion alignment loss \mathcal{L}_{MA} to inject dynamics:

$$\mathcal{L}_{MA} = \sum_{\tau=1}^{\mathcal{T}} \mathcal{L}_{TA}(x_{\theta,\Phi}^{c',\tau}, I_{\text{vid}}^{\tau}) + \sum_{H,W} \|x_{\theta,\Phi}^{c',1} - x_{\theta}^{c',1}\|_2^2. \quad (10)$$

where in the former term, $x_{\theta,\Phi}^{c',\tau}$ is the front-view rendering of θ at time τ , and I_{vid}^{τ} is the τ -frame. For the latter term, dynamic 3DGS and static 3DGS should remain consistent at $\tau = 1$. Thus, we randomly choose a camera view c' and render two images $x_{\theta,\Phi}^{c',1}$ and $x_{\theta}^{c',1}$. We calculate the MSE between them and add it in the Eq. 10.

Reference Refinement. Despite following the aforementioned technical steps to obtain a dynamic, geometrically reasonable 3D target, there are instances where surface splitting may occur. The Gaussian points with predicted locations are too far apart, and the scale cannot bridge the gap between the points. Thus, we propose the reference refinement, which sets the front-view renderings as the pixel reference and applies multiview DMs for inpainting. Different from MVDream [39], which uses text prompt as the condition to generate angle-fixed multiview images, Zero123 [38; 29] supports any poses and one image as inputs to synthesize. Although synthesis doesn’t contain the multiview consistent for 4D generation, the generalization of Zero123 is good enough to inpaint the gap for a smooth surface. Specially, we randomly choose a camera pose c_{ref} and render image $x_{\theta}^{c_{\text{ref}}}$ from static 3D Gaussians θ as the reference to fix 4D rendering $x_{\theta,\Phi}^{c_{\text{ref}},\tau}$ got at timestamp τ . Thus, we propose reference loss \mathcal{L}_{ref} and modify Eq. 2 as follows :

$$\nabla_{\Phi} \mathcal{L}_{\text{ref}}(x = g(\theta, \Phi)) = \mathbb{E}_{t,\epsilon,\tau} \left[w(t) (\hat{\epsilon}_{\phi}(z_{\theta,\Phi}^{c_{\text{ref}},\tau}, z_{\theta}^{c_{\text{ref}}}, c_{\text{ref}}, t) - \epsilon) \frac{\partial x}{\partial \Phi} \right], \quad (11)$$

where $z_{\theta,\Phi}^{c_{\text{ref}},\tau}$ and $z_{\theta}^{c_{\text{ref}}}$ are latents of $x_{\theta,\Phi}^{c_{\text{ref}},\tau}$ and $x_{\theta}^{c_{\text{ref}}}$. With the same viewpoint bias c_{ref} , \mathcal{L}_{ref} pushes deformation net Φ to keep the high-quality surface as the renderings got at time $\tau = 1$. Finally, we can optimize 4D loss $\mathcal{L}_{4D} = \mathcal{L}_{MA} + \mathcal{L}_{\text{ref}}$ for 4D synthesis. Here, \mathcal{L}_{MA} and \mathcal{L}_{ref} counterbalance each other to maintain a balance between motion and surface effects.

4 Experiments

Comparative studies. In Fig. 4, we show and compare the 4D renderings generated by MAV3D, AYG, and PLA4D. PLA4D can generate 4D objects with fine textures, accurate geometry, and coherent motion. In Fig. 4(a), with pixel-level alignments, PLA4D achieves detailed textures and realistic appearances similar to generated images of 2D diffusion models. Additionally, when we

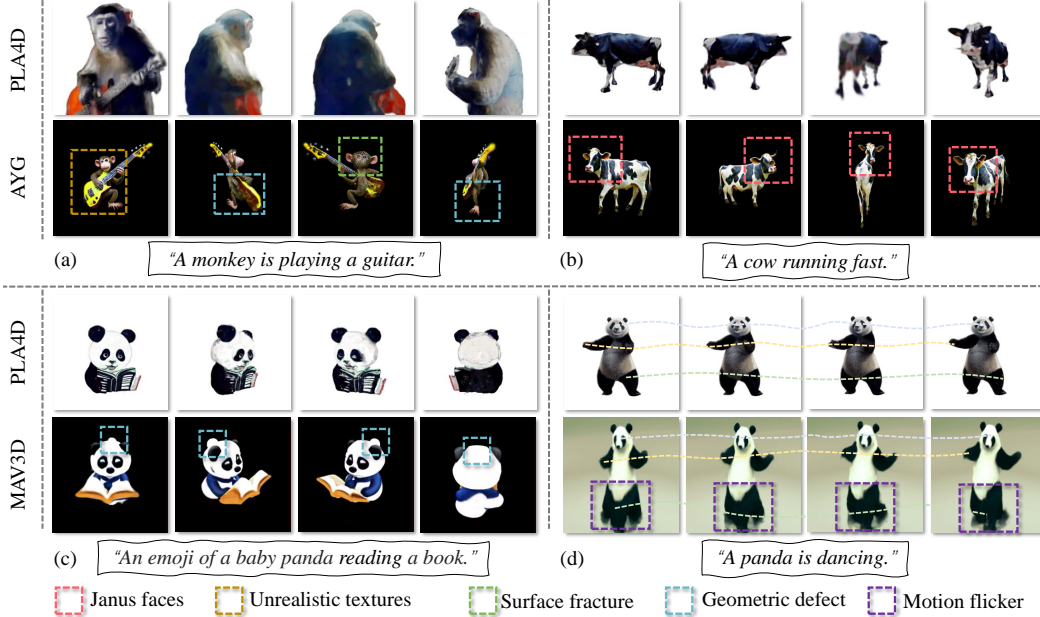


Figure 4: PLA4D generates more realistic targets than MAV3D and AYG by pixel-level alignments. Leveraging the focal alignment method and GS-Mesh contrastive learning, PLA4D effectively avoids multi-head issues (see Subfig.(b)) and potential geometric defects(see Subfig.(a) and Subfig.(c)), thus maintaining excellent geometric configurations. After injecting motion, our proposed motion alignment method effectively prevents short-term motion flicker (see Subfig.(d)), while the reference refinement method prevents surface fracture caused by Gaussian points’ displacement.

Table 1: Comparison among MAV3D, AYG and PLA4D. We recruit 40 volunteers and present the user study results in the middle and report the CLIP cosine similarity between renderings and text prompts on the right.

Methods	Texture(%)	Geometry(%)	Motion(%)	Semantic(%)	CLIP-S(↑)
MAV3D	6.5	12.9	25.6	15.8	0.251
AYG	31.6	25.0	33.0	21.3	0.259
PLA4D (ours)	61.9	62.1	41.4	62.9	0.2688

focus on geometry, it can be observed that PLA4D effectively avoids geometric defects. For example, in In Fig. 4(c), MAV3D incorrectly generates a bulge, while PLA4D produces the correct head shape. Furthermore, the correct geometric information effectively prevents Janus-face problems. As shown in Fig. 4(b), the AYG generation exhibits multiple faces, whereas the PLA4D generation has a single face. When we focus on motion, like the example in Fig. 4(d), PLA4D can reconstruct smooth movements without the flickering seen in MAV3D during short-term continuous changes.

Furthermore, we performed a comprehensive user study following the settings of AYG[27]. We collect the rendered videos from the web pages of MAV3D and AYG, and extract videos from 4D objects generated by PLA4D with the same prompts. Users are asked to cast their votes based on their visual perception in four aspects: texture, geometry, motion, and text-semantic consistency. The results, as shown in Tab. 1, justify PLA4D’s design. Additionally, we introduced CLIP to calculate the cosine similarity between the text and the rendered images to objectively measure the degree of semantic alignment. PLA4D also achieved the highest scores, highlighting the advantages of pixel alignments in our framework.

Ablation Studies. In Fig. 5, we demonstrate the role of each module in PLA4D for text-to-4D generation. First, we remove the focal alignment module. Without the matched focal f , in both frame-to-3D and 3D-to-4D stages, Gaussians can not learn the correct attributes of points to align to the generated frames. The mismatched focal confuses the deformation net and makes it predict many points are transparent. Next, we remove the GS-Mesh contrastive learning module. Despite the

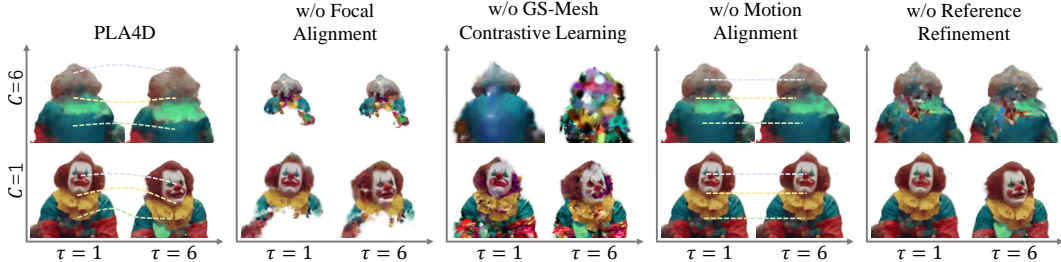


Figure 5: Ablation studies. If no focal alignment or GS-Mesh contrastive learning, the 4D object loses its detailed texture and correct geometry. Without motion alignment, a 4D object degenerates into a static object. Absent reference refinement, the displacement of Gaussians causes surface tearing.

Table 2: Speed comparison. The upper part presents image-to-4D methods, while the lower part collects text-to-4D methods. It can be observed that the less SDS is used during generation, the less time is required for synthesis. Mark * means that SDS is not used in all stages.

Methods	Representation	Generation Time	Iterations	T2I	T2M	T2V
Dream-in-4D [56]	NeRF	10.5 hr	20K	✓	✓	✓*
Animate124 [55]	NeRF	-	20K	✗	✓	✓
Consistent4D [21]	NeRF	2.5 hr	10K	✓	✓	✓
DreamGaussian4D [36]	Gaussians	6.5 min	0.7K	✗	✓*	✓*
4D-fy [3]	NeRF	23 hr	120K	✓	✓	✓
MAV3D [42]	NeRF	6.5 hr	12K	✓	✗	✓
AYG [27]	Gaussians	-	20K	✓	✓	✓
PLA4D (ours)	Gaussians	15 min	1K	✗	✓*	✗

absence of large-scale transparency on the front, numerous floating points detach from the surface. If we look at the back of the 4D object, gaussian points struggle to maintain a consistent volume and instead merely fit the front-rendered images to align with the generated frames. After that, we remove the motion alignment module. The 4D object degrades into a 3D static object. Finally, we demonstrate the effects of removing the reference refinement module. As we mentioned earlier, the displacement of Gaussian points leads to the splitting of the surface. The front-view renderings have corresponding frames to supervise, but the back-view rendered images do not have targets, which causes rendering rays to penetrate the interior of the 4D object through surface crevices.

Efficiency studies. We compare and share the time overhead of multiple 4D generation methods proposed for image-to-4d and text-to-4d tasks, as shown in Tab. 2. It can be observed that previous 4D generation tasks overly rely on SDS, which requires extensive training (over 10K iterations) by implicitly aligning various diffusion models to generate 4D objects. In contrast, PLA4D uses explicit pixel-level alignment, resulting in better textures, geometry, and motion for 4D targets with significantly lower time overhead.

5 Conclusion

In this paper, we introduce PLA4D, a framework that leverages text-driven generated video as explicit pixel alignment targets for 4D synthesis. Our approach incorporates GS-Mesh contrastive learning and focal alignment, which ensures geometry consistency from the mesh and produces textures as detailed as those in the generated video frames. Additionally, we have developed a novel motion alignment method and reference refinement technology to optimize dynamic surfaces. Compared to existing methods, PLA4D effectively avoids multi-head issues and generates 4D targets with rich textures, accurate geometry, and smooth motion in significantly less time. Furthermore, PLA4D is constructed entirely using existing open-source models, eliminating the need for pre-training any diffusion models. This flexible architecture allows the community to freely replace or upgrade components to achieve state-of-the-art performance. We aim for PLA4D to become an accessible, user-friendly, and promising tool for 4D digital content creation.

References

- [1] Jie An, Songyang Zhang, Harry Yang, Sonal Gupta, Jia-Bin Huang, Jiebo Luo, and Xi Yin. Latent-shift: Latent diffusion with temporal shift for efficient text-to-video generation. *arXiv preprint arXiv:2304.08477*, 2023.
- [2] Vladimir Arkhipkin, Zein Shaheen, Viacheslav Vasilev, Elizaveta Dakhova, Andrey Kuznetsov, and Denis Dimitrov. Fusionframes: Efficient architectural aspects for text-to-video generation pipeline. *arXiv preprint arXiv:2311.13073*, 2023.
- [3] Sherwin Bahmani, Ivan Skorokhodov, Victor Rong, Gordon Wetzstein, Leonidas Guibas, Peter Wonka, Sergey Tulyakov, Jeong Joon Park, Andrea Tagliasacchi, and David B Lindell. 4d-fy: Text-to-4d generation using hybrid score distillation sampling. *arXiv preprint arXiv:2311.17984*, 2023.
- [4] Andreas Blattmann, Tim Dockhorn, Sumith Kulal, Daniel Mendelevitch, Maciej Kilian, Dominik Lorenz, Yam Levi, Zion English, Vikram Voleti, Adam Letts, et al. Stable video diffusion: Scaling latent video diffusion models to large datasets. *arXiv preprint arXiv:2311.15127*, 2023.
- [5] Andreas Blattmann, Robin Rombach, Huan Ling, Tim Dockhorn, Seung Wook Kim, Sanja Fidler, and Karsten Kreis. Align your latents: High-resolution video synthesis with latent diffusion models. In *Proceedings of the IEEE/CVF Conference on Computer Vision and Pattern Recognition*, pages 22563–22575, 2023.
- [6] Ang Cao and Justin Johnson. Hexplane: A fast representation for dynamic scenes. In *Proceedings of the IEEE/CVF Conference on Computer Vision and Pattern Recognition*, pages 130–141, 2023.
- [7] Guikun Chen and Wenguan Wang. A survey on 3d gaussian splatting. *arXiv preprint arXiv:2401.03890*, 2024.
- [8] Rui Chen, Yongwei Chen, Ningxin Jiao, and Kui Jia. Fantasia3d: Disentangling geometry and appearance for high-quality text-to-3d content creation. In *Proceedings of the IEEE/CVF International Conference on Computer Vision*, pages 22246–22256, 2023.
- [9] Yiwen Chen, Chi Zhang, Xiaofeng Yang, Zhongang Cai, Gang Yu, Lei Yang, and Guosheng Lin. IT3D: improved text-to-3d generation with explicit view synthesis. In Michael J. Wooldridge, Jennifer G. Dy, and Sriraam Natarajan, editors, *Thirty-Eighth AAAI Conference on Artificial Intelligence, AAAI 2024, Thirty-Sixth Conference on Innovative Applications of Artificial Intelligence, IAAI 2024, Fourteenth Symposium on Educational Advances in Artificial Intelligence, EAAI 2014, February 20-27, 2024, Vancouver, Canada*, pages 1237–1244. AAAI Press, 2024.
- [10] Matt Deitke, Ruoshi Liu, Matthew Wallingford, Huong Ngo, Oscar Michel, Aditya Kusupati, Alan Fan, Christian Laforte, Vikram Voleti, Samir Yitzhak Gadre, et al. Objaverse-xl: A universe of 10m+ 3d objects. *Advances in Neural Information Processing Systems*, 36, 2024.
- [11] Matt Deitke, Dustin Schwenk, Jordi Salvador, Luca Weihs, Oscar Michel, Eli VanderBilt, Ludwig Schmidt, Kiana Ehsani, Aniruddha Kembhavi, and Ali Farhadi. Objaverse: A universe of annotated 3d objects. In *Proceedings of the IEEE/CVF Conference on Computer Vision and Pattern Recognition*, pages 13142–13153, 2023.
- [12] Congyue Deng, Chiyu Jiang, Charles R Qi, Xinchun Yan, Yin Zhou, Leonidas Guibas, Dragomir Anguelov, et al. NERDI: Single-view nerf synthesis with language-guided diffusion as general image priors. In *Proceedings of the IEEE/CVF Conference on Computer Vision and Pattern Recognition*, pages 20637–20647, 2023.
- [13] Lincong Feng, Muyu Wang, Maoyu Wang, Kuo Xu, and Xiaoli Liu. Metadreamer: Efficient text-to-3d creation with disentangling geometry and texture. *arXiv preprint arXiv:2311.10123*, 2023.
- [14] Songwei Ge, Seungjun Nah, Guilin Liu, Tyler Poon, Andrew Tao, Bryan Catanzaro, David Jacobs, Jia-Bin Huang, Ming-Yu Liu, and Yogesh Balaji. Preserve your own correlation: A noise prior for video diffusion models. In *Proceedings of the IEEE/CVF International Conference on Computer Vision*, pages 22930–22941, 2023.

- [15] Rohit Girdhar, Mannat Singh, Andrew Brown, Quentin Duval, Samaneh Azadi, Sai Saketh Rambhatla, Akbar Shah, Xi Yin, Devi Parikh, and Ishan Misra. Emu video: Factorizing text-to-video generation by explicit image conditioning. *arXiv preprint arXiv:2311.10709*, 2023.
- [16] Yuwei Guo, Ceyuan Yang, Anyi Rao, Yaohui Wang, Yu Qiao, Dahua Lin, and Bo Dai. AnimateDiff: Animate your personalized text-to-image diffusion models without specific tuning. *arXiv preprint arXiv:2307.04725*, 2023.
- [17] Jonathan Ho, William Chan, Chitwan Saharia, Jay Whang, Ruiqi Gao, Alexey Gritsenko, Diederik P Kingma, Ben Poole, Mohammad Norouzi, David J Fleet, et al. Imagen video: High definition video generation with diffusion models. *arXiv preprint arXiv:2210.02303*, 2022.
- [18] Jonathan Ho and Tim Salimans. Classifier-free diffusion guidance. *arXiv preprint arXiv:2207.12598*, 2022.
- [19] Hugues Hoppe, Tony DeRose, Tom Duchamp, John McDonald, and Werner Stuetzle. Mesh optimization. In *Proceedings of the 20th annual conference on Computer graphics and interactive techniques*, pages 19–26, 1993.
- [20] Yukun Huang, Jianan Wang, Yukai Shi, Xianbiao Qi, Zheng-Jun Zha, and Lei Zhang. DreamTime: An improved optimization strategy for text-to-3d content creation. *arXiv preprint arXiv:2306.12422*, 2023.
- [21] Yanqin Jiang, Li Zhang, Jin Gao, Weimin Hu, and Yao Yao. Consistent4d: Consistent 360 $\{\backslash\deg\}$ dynamic object generation from monocular video. *arXiv preprint arXiv:2311.02848*, 2023.
- [22] Oren Katzir, Or Patashnik, Daniel Cohen-Or, and Dani Lischinski. Noise-free score distillation. *arXiv preprint arXiv:2310.17590*, 2023.
- [23] Bernhard Kerbl, Georgios Kopanas, Thomas Leimkühler, and George Drettakis. 3d gaussian splatting for real-time radiance field rendering. *ACM Transactions on Graphics*, 42(4):1–14, 2023.
- [24] Levon Khachatryan, Andranik Movsisyan, Vahram Tadevosyan, Roberto Henschel, Zhangyang Wang, Shant Navasardyan, and Humphrey Shi. Text2video-zero: Text-to-image diffusion models are zero-shot video generators. In *Proceedings of the IEEE/CVF International Conference on Computer Vision*, pages 15954–15964, 2023.
- [25] Yixun Liang, Xin Yang, Jiantao Lin, Haodong Li, Xiaogang Xu, and Yingcong Chen. LucidDreamer: Towards high-fidelity text-to-3d generation via interval score matching. *arXiv preprint arXiv:2311.11284*, 2023.
- [26] Chen-Hsuan Lin, Jun Gao, Luming Tang, Towaki Takikawa, Xiaohui Zeng, Xun Huang, Karsten Kreis, Sanja Fidler, Ming-Yu Liu, and Tsung-Yi Lin. Magic3d: High-resolution text-to-3d content creation. In *Proceedings of the IEEE/CVF Conference on Computer Vision and Pattern Recognition*, pages 300–309, 2023.
- [27] Huan Ling, Seung Wook Kim, Antonio Torralba, Sanja Fidler, and Karsten Kreis. Align your gaussians: Text-to-4d with dynamic 3d gaussians and composed diffusion models. *arXiv preprint arXiv:2312.13763*, 2023.
- [28] Minghua Liu, Chao Xu, Haiyan Jin, Linghao Chen, Mukund Varma T, Zexiang Xu, and Hao Su. One-2-3-45: Any single image to 3d mesh in 45 seconds without per-shape optimization. *Advances in Neural Information Processing Systems*, 36, 2024.
- [29] Ruoshi Liu, Rundi Wu, Basile Van Hoorick, Pavel Tokmakov, Sergey Zakharov, and Carl Vondrick. Zero-1-to-3: Zero-shot one image to 3d object. In *Proceedings of the IEEE/CVF International Conference on Computer Vision*, pages 9298–9309, 2023.
- [30] Yuan Liu, Cheng Lin, Zijiao Zeng, Xiaoxiao Long, Lingjie Liu, Taku Komura, and Wenping Wang. SyncDreamer: Generating multiview-consistent images from a single-view image. *arXiv preprint arXiv:2309.03453*, 2023.

- [31] Jonathan Lorraine, Kevin Xie, Xiaohui Zeng, Chen-Hsuan Lin, Towaki Takikawa, Nicholas Sharp, Tsung-Yi Lin, Ming-Yu Liu, Sanja Fidler, and James Lucas. Att3d: Amortized text-to-3d object synthesis. In *Proceedings of the IEEE/CVF International Conference on Computer Vision*, pages 17946–17956, 2023.
- [32] Ben Mildenhall, Pratul P Srinivasan, Matthew Tancik, Jonathan T Barron, Ravi Ramamoorthi, and Ren Ng. Nerf: Representing scenes as neural radiance fields for view synthesis. *Communications of the ACM*, 65(1):99–106, 2021.
- [33] Keunhong Park, Utkarsh Sinha, Jonathan T Barron, Sofien Bouaziz, Dan B Goldman, Steven M Seitz, and Ricardo Martin-Brualla. Nerfies: Deformable neural radiance fields. In *Proceedings of the IEEE/CVF International Conference on Computer Vision*, pages 5865–5874, 2021.
- [34] Ben Poole, Ajay Jain, Jonathan T Barron, and Ben Mildenhall. Dreamfusion: Text-to-3d using 2d diffusion. *arXiv preprint arXiv:2209.14988*, 2022.
- [35] Albert Pumarola, Enric Corona, Gerard Pons-Moll, and Francesc Moreno-Noguer. D-nerf: Neural radiance fields for dynamic scenes. In *Proceedings of the IEEE/CVF Conference on Computer Vision and Pattern Recognition*, pages 10318–10327, 2021.
- [36] Jiawei Ren, Liang Pan, Jiaxiang Tang, Chi Zhang, Ang Cao, Gang Zeng, and Ziwei Liu. Dreamgaussian4d: Generative 4d gaussian splatting. *arXiv preprint arXiv:2312.17142*, 2023.
- [37] Robin Rombach, Andreas Blattmann, Dominik Lorenz, Patrick Esser, and Björn Ommer. High-resolution image synthesis with latent diffusion models. In *Proceedings of the IEEE/CVF conference on computer vision and pattern recognition*, pages 10684–10695, 2022.
- [38] Ruoxi Shi, Hansheng Chen, Zhuoyang Zhang, Minghua Liu, Chao Xu, Xinyue Wei, Linghao Chen, Chong Zeng, and Hao Su. Zero123++: a single image to consistent multi-view diffusion base model. *arXiv preprint arXiv:2310.15110*, 2023.
- [39] Yichun Shi, Peng Wang, Jianglong Ye, Mai Long, Kejie Li, and Xiao Yang. Mvdream: Multi-view diffusion for 3d generation. *arXiv preprint arXiv:2308.16512*, 2023.
- [40] Karen Simonyan and Andrew Zisserman. Very deep convolutional networks for large-scale image recognition. *arXiv preprint arXiv:1409.1556*, 2014.
- [41] Uriel Singer, Adam Polyak, Thomas Hayes, Xi Yin, Jie An, Songyang Zhang, Qiyuan Hu, Harry Yang, Oron Ashual, Oran Gafni, et al. Make-a-video: Text-to-video generation without text-video data. *arXiv preprint arXiv:2209.14792*, 2022.
- [42] Uriel Singer, Shelly Sheynin, Adam Polyak, Oron Ashual, Iurii Makarov, Filippos Kokkinos, Naman Goyal, Andrea Vedaldi, Devi Parikh, Justin Johnson, et al. Text-to-4d dynamic scene generation. *arXiv preprint arXiv:2301.11280*, 2023.
- [43] Jingxiang Sun, Bo Zhang, Ruizhi Shao, Lizhen Wang, Wen Liu, Zhenda Xie, and Yebin Liu. Dreamcraft3d: Hierarchical 3d generation with bootstrapped diffusion prior. *arXiv preprint arXiv:2310.16818*, 2023.
- [44] Jiaxiang Tang. Stable-dreamfusion: Text-to-3d with stable-diffusion. *Stable-dreamfusion: Text-to-3d with stable-diffusion*, 2022.
- [45] Jiaxiang Tang, Jiawei Ren, Hang Zhou, Ziwei Liu, and Gang Zeng. Dreamgaussian: Generative gaussian splatting for efficient 3d content creation. *arXiv preprint arXiv:2309.16653*, 2023.
- [46] Christina Tsalicoglou, Fabian Manhardt, Alessio Tonioni, Michael Niemeyer, and Federico Tombari. Textmesh: Generation of realistic 3d meshes from text prompts. *arXiv preprint arXiv:2304.12439*, 2023.
- [47] Haochen Wang, Xiaodan Du, Jiahao Li, Raymond A Yeh, and Greg Shakhnarovich. Score jacobian chaining: Lifting pretrained 2d diffusion models for 3d generation. In *Proceedings of the IEEE/CVF Conference on Computer Vision and Pattern Recognition*, pages 12619–12629, 2023.

- [48] Haochen Wang, Xiaodan Du, Jiahao Li, Raymond A Yeh, and Greg Shakhnarovich. Score jacobian chaining: Lifting pretrained 2d diffusion models for 3d generation. In *Proceedings of the IEEE/CVF Conference on Computer Vision and Pattern Recognition*, pages 12619–12629, 2023.
- [49] Wenjing Wang, Huan Yang, Zixi Tuo, Huiguo He, Junchen Zhu, Jianlong Fu, and Jiaying Liu. Videofactory: Swap attention in spatiotemporal diffusions for text-to-video generation. *arXiv preprint arXiv:2305.10874*, 2023.
- [50] Yaohui Wang, Xinyuan Chen, Xin Ma, Shangchen Zhou, Ziqi Huang, Yi Wang, Ceyuan Yang, Yinan He, Jiashuo Yu, Peiqing Yang, et al. Lavie: High-quality video generation with cascaded latent diffusion models. *arXiv preprint arXiv:2309.15103*, 2023.
- [51] Zhengyi Wang, Cheng Lu, Yikai Wang, Fan Bao, Chongxuan Li, Hang Su, and Jun Zhu. Prolicfdreamer: High-fidelity and diverse text-to-3d generation with variational score distillation. *Advances in Neural Information Processing Systems*, 36, 2024.
- [52] Zhengyi Wang, Yikai Wang, Yifei Chen, Chendong Xiang, Shuo Chen, Dajiang Yu, Chongxuan Li, Hang Su, and Jun Zhu. Crm: Single image to 3d textured mesh with convolutional reconstruction model. *arXiv preprint arXiv:2403.05034*, 2024.
- [53] Xin Yu, Yuan-Chen Guo, Yangguang Li, Ding Liang, Song-Hai Zhang, and Xiaojuan Qi. Text-to-3d with classifier score distillation. *arXiv preprint arXiv:2310.19415*, 2023.
- [54] Richard Zhang, Phillip Isola, Alexei A Efros, Eli Shechtman, and Oliver Wang. The unreasonable effectiveness of deep features as a perceptual metric. In *Proceedings of the IEEE conference on computer vision and pattern recognition*, pages 586–595, 2018.
- [55] Yuyang Zhao, Zhiwen Yan, Enze Xie, Lanqing Hong, Zhenguo Li, and Gim Hee Lee. Animate124: Animating one image to 4d dynamic scene. *arXiv preprint arXiv:2311.14603*, 2023.
- [56] Yufeng Zheng, Xueting Li, Koki Nagano, Sifei Liu, Otmar Hilliges, and Shalini De Mello. A unified approach for text-and image-guided 4d scene generation. *arXiv preprint arXiv:2311.16854*, 2023.
- [57] Matthias Zwicker, Hanspeter Pfister, Jeroen Van Baar, and Markus Gross. Ewa volume splatting. In *Proceedings Visualization, 2001. VIS'01.*, pages 29–538. IEEE, 2001.

A Implementation Details

A.1 Important Details

Our setup includes an AMD EPYC 7313 16-core Processor for the CPU, 256GB of memory, and 4 Nvidia RTX 4090 GPUs. In the text-to-video stage, we use KandiskyVideo [2] and load each submodule of in each GPU for VRAM load balancing. We set the width and height of generated frames as 512 with 8 frames. Next, we use the rembg tool² to get the foreground. For frame-to-3D synthesis, we use the foreground of the first frame as the reference and send it into CRM [52] to get the mesh during 50 denoising steps. Next, we run 1000 iterations with a batch size of 6. The init focal is 49.1 following the settings of Zero-1-to-3 [29; 38]. We linearly decay λ_t from 0.98 to 0.02. For 4D representation, we run 65 iterations with batch size 6, with λ_t linearly decaying from 0.5 to 0.02 following DreamGaussian4D [36].

A.2 Rendering Resolution

In the initial 3D synthesis stage, we render scenes at a resolution of 128×128. When training reaches the halfway point, we increase the rendering resolution to 256×256. Subsequently, when the training phase reaches 70%, we further elevate the rendering resolution to 512×512. The same strategy is employed in the main 4D synthesis stage.

B More Results

B.1 Prompts

We used all the 28 prompts from MAV3D’s project page: “An alien playing the piano.”; “Shark swimming in the desert.”; “A dog wearing a Superhero outfit with red cape flying through the sky.”; “A monkey eating a candy bar.”; “A squirrel DJing.”; “A cat singing.”; “A bear driving a car.”; “Chihuahua running on the grass.”; “A human skeleton drinking wine.”; “A yorkie dog eating a donut”; “A baby panda eating ice cream”; “A kangaroo cooking a meal.”; “A humanoid robot playing the violin.”; “A squirrel playing the saxophone.”;

For the ablation study, we selected the following 30 text prompts: “An octopus is underwater.”; “A silver humanoid robot flipping a coin.”; “A goat drinking beer.”; “A squirrel playing on a swing set.”; “A panda playing on a swing set.”; “A crocodile playing a drum set.”; “A squirrel riding a motorcycle.”; “3D rendering of a fox playing videogame.”; “A dog riding a skateboard.”; “An emoji of a baby panda reading a book.”; “Clown fish swimming through the coral reef.”; “A space shuttle launching.”; “A corgi playing with a ball.”; “A panda dancing.” For the ablation study, we selected the following 30 text prompts: “A cat singing.”; “A corgi playing with a ball.”; “A cow running fast.”; “A dog wearing a Superhero outfit with red cape flying through the sky.”; “A fox dressed in a suit dancing.”; “A monkey eating a candy bar.”; “A monkey is playing bass guitar.”; “A panda dancing.”; “A panda surfing a wave.”; “A pig running fast.”; “A purple unicorn flying.”; “A space shuttle launching.”; “A squirrel DJing.”; “A squirrel playing on a swing set.”; “A squirrel playing the saxophone.”; “A squirrel riding a motorcycle.”; “A storm trooper walking forward and vacuuming.”; “An alien playing the piano.”; “an astronaut is playing the electric guitar.”; “An astronaut riding a horse.”; “An astronaut riding motorcycle.”; “A panda reading a book.”; “Beer pouring into a glass.”; “Chihuahua running.”; “Clown fish swimming.”; “A dog riding a skateboard.”; “Flying dragon on fire.”; “Intricate butterfly flutters its wings.”; “Waves crashing against a lighthouse.”; “Wood on fire.”

B.2 Visual Results

²<https://github.com/danielgatis/rembg>



Figure 6: 4D rendering results.

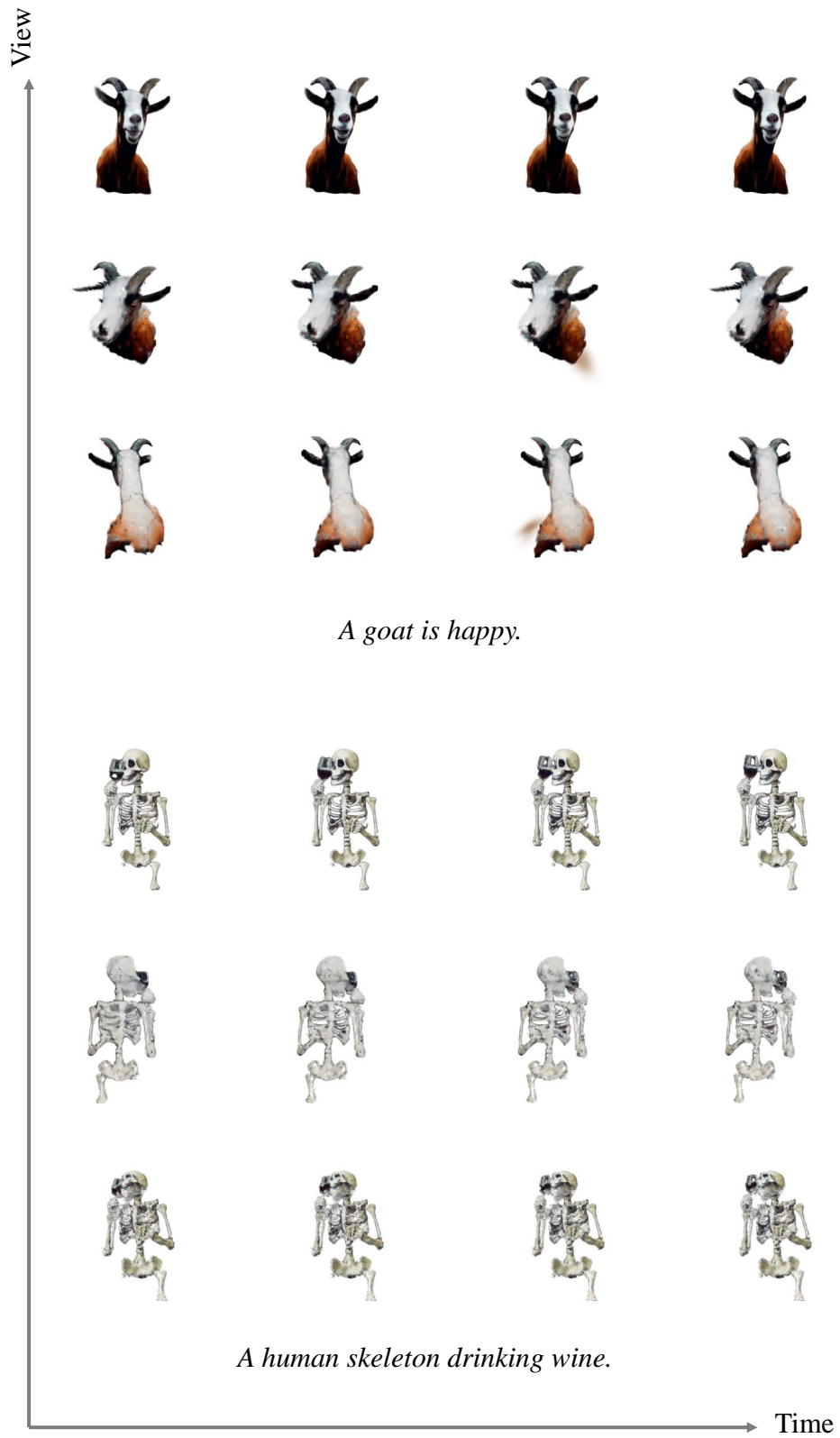


Figure 7: 4D rendering results.

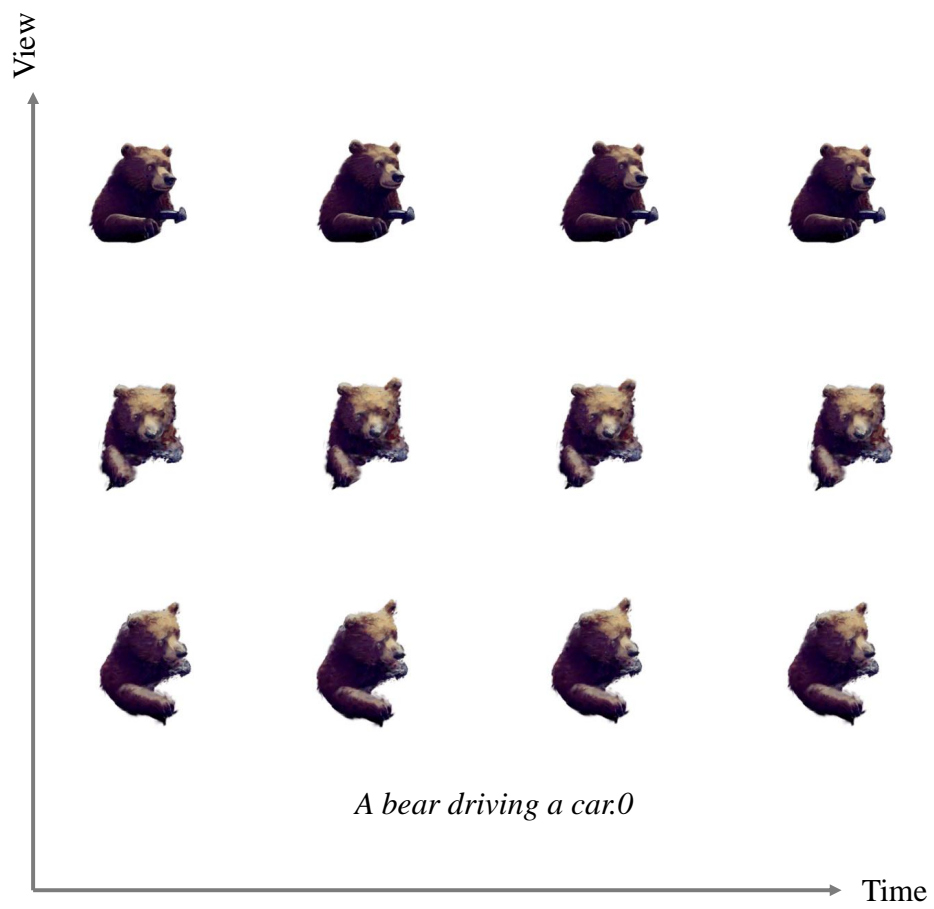


Figure 8: 4D rendering results

C Pseudocode of PLA4D

Here, we provide the pseudocode for the two stages in PLA4D: frame-to-3D and 3D-to-4D.

Algorithm 1: Frame-to-3D Generation

Input: First frame I_{vid}^1 , epoch E , Image-to-Mesh diffusion model G_ψ ,

Output: Static 3D Gaussians representation θ ,

init 3D Gaussians θ ;

get mesh $\psi \leftarrow G_\psi(I_{\text{vid}}^1)$;

search focal f by focal alignment method;

for $e \leftarrow 1$ **to** E **do**

 get front-view rendering $x_\theta^c \leftarrow g(\theta)$;

$\mathcal{L}_{\text{MSE}} \leftarrow \text{MSE}(x_\theta^c, I_{\text{vid}}^1)$;

$\mathcal{L}_{\text{Mask}} \leftarrow \text{MSE}(\alpha_\theta^c, \alpha_{\text{vid}}^1)$;

$\mathcal{L}_{\text{LPIPS}} \leftarrow \text{MSE}(z_\theta^c, z_{\text{vid}}^1)$;

$\mathcal{L}_{\text{TA}} \leftarrow \lambda_t \mathcal{L}_{\text{MSE}} + \lambda_t \mathcal{L}_{\text{Mask}} + \gamma \mathcal{L}_{\text{LPIPS}}$;

for $i \leftarrow 1$ **to** 6 **do**

 get random view c' ;

 render image $x_\theta^{c'} \leftarrow g_\theta(c')$;

 render image $x_\psi^{c'} \leftarrow g_\psi(c')$;

$\mathcal{L}_{\text{MSE}}^i \leftarrow \text{MSE}(x_\theta^{c'}, x_\psi^{c'})$;

$\mathcal{L}_{\text{Mask}}^i \leftarrow \text{MSE}(\alpha_\theta^{c'}, \alpha_\psi^{c'})$;

$\mathcal{L}_{\text{LPIPS}}^i \leftarrow \text{MSE}(z_\theta^{c'}, z_\psi^{c'})$;

$\mathcal{L}_{\text{GA}}^i \leftarrow \lambda_i \mathcal{L}_{\text{MSE}} + \lambda_t \mathcal{L}_{\text{Mask}}^i + \gamma \mathcal{L}_{\text{LPIPS}}^i$;

$\mathcal{L}_{\text{GA}} \leftarrow \mathcal{L}_{\text{GA}} + \mathcal{L}_{\text{GA}}^i$;

end

$\mathcal{L}_{3\text{D}} = \mathcal{L}_{\text{TA}} + \mathcal{L}_{\text{GA}}$;

 Optimize and update θ ;

end

return θ ;

Algorithm 2: 3D-to-4D Generation

Input: Generated video $\{I_{\text{vid}}^\tau\}_{\mathcal{T}}$, epoch E , Static 3D Gaussians θ , Frame number \mathcal{T}

Output: Deformation net Φ ,

search focal f by focal alignment method;

for $e \leftarrow 1$ **to** E **do**

for $\tau \leftarrow 1$ **to** \mathcal{T} **do**

 get front-view rendering $x_{\theta, \Phi}^{c, \tau} \leftarrow g(\theta, \Phi)$;

$\mathcal{L}_{\text{MSE}} \leftarrow \text{MSE}(x_{\theta, \Phi}^{c, \tau}, I_{\text{vid}}^\tau)$;

$\mathcal{L}_{\text{Mask}} \leftarrow \text{MSE}(\alpha_{\theta, \Phi}^{c, \tau}, \alpha_{\text{vid}}^\tau)$;

$\mathcal{L}_{\text{LPIPS}} \leftarrow \text{MSE}(z_{\theta, \Phi}^{c, \tau}, z_{\text{vid}}^\tau)$;

$\mathcal{L}_{\text{MA}} \leftarrow \mathcal{L}_{\text{MA}} + \lambda_t \mathcal{L}_{\text{MSE}} + \lambda_t \mathcal{L}_{\text{Mask}} + \gamma \mathcal{L}_{\text{LPIPS}}$;

for $i \leftarrow 1$ **to** 2 **do**

 get random view c' ;

 render image $x_\theta^{c'}$ $\leftarrow g(\theta)$;

 render image $x_{\theta, \Phi}^{c', \tau} \leftarrow g(\theta, \Phi)$;

$\mathcal{L}_{\text{ref}} = \text{SDS}(x_{\theta, \Phi}^{c', \tau}, x_\theta^{c'}, c')$

end

end

 get random-view rendering $x_\theta^{c'}$ $\leftarrow g(\theta)$;

 get random-view rendering $x_{\theta, \Phi}^{c', \tau} \leftarrow g(\theta, \Phi)$;

$\mathcal{L}_{\text{MA}} \leftarrow \mathcal{L}_{\text{MA}} + \text{MSE}(x_{\theta, \Phi}^{c', \tau}, x_\theta^{c'})$;

$\mathcal{L}_{\text{4D}} = \mathcal{L}_{\text{ref}} + \mathcal{L}_{\text{MA}}$;

 Optimize and update Φ ;

end

return θ ;

D Limitations

Although the PLA4D model fully leverages existing diffusion models for direct generation, it also has several limitations. Constrained by the performance of current open-source text-to-image generation models, the generated videos often exhibit limited motion range. The potential of the model could be further realized with the advent of higher-quality video generation models. Additionally, the image-to-mesh model is limited by its own generative capabilities and cannot reconstruct all targets, necessitating further research by the relevant scientific community.